LA-UR-21-21481
Approved for public release; distribution is unlimited.

Title: 2D Simulations of Diamagnetic Loop Calibrations

Author(s): Ekdahl, Carl August Jr.
Broste, William B
Smith, Horace Vernon

Intended for: Report

Issued: 2021-02-17

2D Simulations of Diamagnetic Loop Calibrations

Carl Ekdahl, William B. Broste, and H. Vernon Smith

***Abstract*—Diamagnetic loops can be used as a non-invasive method for measurements of beam size in electron beam accelerators that use solenoidal magnetic transport. A comprehensive theory for interpreting data from a diamagnetic loop relates the rms beam radius to the excluded flux measured by the loop and the beam current. Thus, primary calibration of the loop must relate the loop signal directly to the excluded flux. We have simulated these calibrations with a 2D field solver in order to identify possible sources of uncertainty in our calibration technique.**

***Index Terms*—Linear induction accelerator, accelerator diagnostics, beam diagnostics**

I. Introduction

THE diamagnetic loop diagnostic technique fundamentally measures the magnetic flux excluded by a diamagnetic object. The excluded flux measurement is then related to some physical property of the object through a model; perhaps with the help of additional measurements from other diagnostics. Whether the final result is the energy of a plasma column [1], the size of a charged-particle beam [2], the velocity of a metal projectile or jet, or the susceptibility of a diamagnetic salt, the uncertainty of the result directly depends on the accuracy of the excluded flux measurement. Therefore, primary calibration must also be directly in terms of the excluded flux, rather than a physical property of the diamagnetic object that is inferred through a model and auxiliary measurements. In this way, the fundamental calibration is free of any assumptions and approximations made in relating material properties to the excluded flux.

The diamagnetic loop (DML) technique consists of filling the experimental volume with a magnetic field, and measuring the change in flux through a loop when a diamagnetic object is introduced. In particular, DMLs have been used to measure the size of intense, relativistic electron beams (IREBs) [2, 3, 4]. Although DML measurements have been made in a bewildering variety of geometries for magnetized-plasma experiments, the geometry for IREB measurements is usually axisymmetric, which greatly simplifies the problem, and lends itself to 2D simulations.

This article gives an overview of the technique and a prototype DML apparatus under development at Los Alamos for proof-of-principle testing with an IREB. In what follows, we briefly discuss the theory, DML apparatus, calibration method, and 2D simulations of the calibration.

II. Theory

In its simplest form, the DML technique is illustrated in Fig. 1. A very long conducting beam pipe with radius R_W initially contains a uniform axial magnetic field B_0. Introduction of an electron beam pulse depresses the field inside the beam. The field outside of the beam is increased by an increment, ΔB, in order to conserve flux inside of the pipe. Flux is only conserved for a short time determined by the magnetic penetration time of the conducting pipe. However, for our purposes, we confine the discussion to considerations of a simple cylindrical geometry with a uniform magnetic field. We also assume azimuthal symmetry to the diamagnetic object, and that it is much longer than any of the radial dimensions so that we may ignore axial variations in what follows.

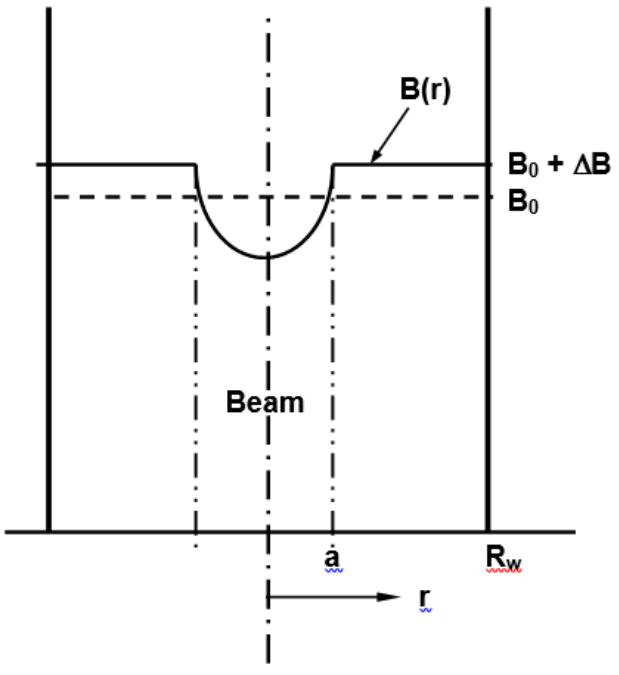

Fig. 1: Magnetic fields inside diamagnetic loop diagnostic. B_0 is the field prior to arrival of the beam. The field is depressed inside the

beam by its diamagnetism. Outside of the beam, the field is increased by ΔB in order to conserve flux. (Adapted from ref. [5])

Consider a single loop with radius R_L and area $A_L = \pi R_L^2$ centered within a cylindrical vessel with radius R_W and area $A_W = \pi R_W^2$. The vessel may, or may not, be a conductor that conserves rapid changes of flux. Also, suppose that the vessel is filled with a uniform axial magnetic field B_0 Now introduce a diamagnetic object as shown in Fig. 1. In our case, the object is a charged particle beam, but it could also be a plasma column, a bullet fired from a gun, or a diamagnetic salt. Inside the object, the field decreases due to diamagnetism. Outside the object the field increases to conserve flux.

A. *Excluded Flux*

The flux excluded from the object is defined as [1]

$$\Phi_x \equiv \left(B_0 + \Delta B\right) A_a - \int_0^a B_z(r) 2\pi r dr \tag{1}$$

where $A_i = \pi R_i^2$ [1]. From flux conservation one has

$$B_0 A_W = \left(B_0 + \Delta B\right)\left(A_W - A_a\right) + \int_0^a B_z(r) 2\pi r dr \tag{2}$$

which simplifies to

$$\Phi_x = \Delta B A_W \tag{3}$$

We measure the change in flux through a DL surrounding the object, which is

$$\Delta\Phi_L = \left(B_0 + \Delta B\right)\left(A_L - A_a\right) + \int_0^a B_z(r) 2\pi r dr - B_0 A_L \tag{4}$$

which simplifies to

$$\Delta\Phi_L = \Delta B A_L - \Phi_x \tag{5}$$

Using Eq. (3) one has

$$\Delta\Phi_L = -\left(1 - A_L / A_W\right)\Phi_x \tag{6}$$

It remains to relate the excluded flux to a model of the object.

B. *Rigid Rotor Excluded Flux*

The relation between parameters and excluded flux can be deduced from the rigid-rotor beam equilibrium [6, 7, 8]. In order to conserve angular momentum, a beam born without any at a shielded cathode must rotate when it subsequently enters an axial magnetic field. Consider a uniform beam with current I_b and radius a rigidly rotating in an axial magnetic field B_z. Conservation of canonical angular momentum gives the angular frequency:

$$P_\theta = \gamma m_e a^2 \omega - e a^2 B_z / 2 \tag{7}$$

For the DARHT beam born in a shielded diode, $P_\theta = 0$, so

$$\omega = \frac{eB_z}{2\gamma m_e} \tag{8}$$

which is just the betatron frequency. In practical units $\omega = ck_\beta = c(cm/s)B_z(kG)/3.4\gamma$. Therefore, the azimuthal current density in the beam is

$$j_\theta = nev_\theta == ner\omega \tag{9}$$

where the density is a constant $ne = J_z / \beta c$. Taking the beam to be infinitely long compared to the DL apparatus, one can calculate the diamagnetic magnetic field inside a shell of thickness dr to be

$$dB_D = \mu_0 j_\theta dr \tag{10}$$

giving

$$B_D = -\mu_0 \frac{\omega J_z}{\beta c}\int_0^r r dr = -\mu_0 \frac{\omega J_z r^2}{2\beta c} \tag{11}$$

Integrating this field over the beam area gives the flux excluded by the rotating beam,

$$\Phi_x = -\mu_0 \frac{\omega J_z}{2\beta c}\int_0^a r^2 2\pi r dr \tag{12}$$

Integrating, one gets

$$\begin{aligned}\Phi_x &= -\mu_0 \frac{\omega J_z \pi a^4}{4\beta c} \\ &= -\mu_0 \frac{\omega a^2 I_b}{4\beta c} \\ &= -\mu_0 \frac{eB_z}{2m_e c\beta\gamma}\frac{I_b a^2}{4} \\ &= -\frac{I_b}{2I_A}\pi a^2 B_z\end{aligned} \tag{13}$$

where equilibrium beam rotation at the betatron frequency has been used, and $I_A = \frac{4\pi}{\mu_0}\frac{m_e c}{e}\beta\gamma = 17.05\beta\gamma$ kA is the Alfven limiting current.

Thus, one has the beam radius in terms of the measured excluded flux and known B_z, I_b, and γ;

$$\pi a^2 = -\frac{2I_A}{I_b}\frac{\Phi_x}{B_z} \tag{14}$$

where Φ_x is related to the diamagnetic loop measurement by Eq. (6). This is the same as Eq. (48) in ref. [5], which was derived more rigorously for an arbitrary axisymmetric current distribution. Since it has been derived for a cold IREB, it does not include the additional diamagnetic contribution due to beam temperature/emittance [9]. Although the correction for this is expected to be inconsequential for DARHT-like beams,

it will be examined in a future article.

III. Apparatus

According to Eq. (13), the largest DML signals (lowest S/N ratio) will be obtained for large high-current, low-energy beams in a strong magnetic field. The only control the experimenter has over this is the bias magnetic field, so our apparatus is incorporates a dedicated solenoid to provide the bias field, rather than relying on the fringe field of existing transport solenoids. Among other advantages, this permits flexible selection of placement of the DML in drift regions.. In use as an installed beam monitor, the DML solenoid can be integrated into the overall magnetic transport tune once it has been adjusted to provide adequate DML signal amplitude.

An advantage of incorporating a dedicated bias solenoid is that it permits enlarging the detection area, which is the area between the loop and the wall, as clear from Eq. (6). Thus, our apparatus has an outer wall diameter of about twice the DML diameter, which was not possible in previous attempts on DARHT-II.

A. Dimensions

Fig. 2 is an illustration of our prototype DML apparatus as it might be installed in the beam line of DARHT or Scorpius. Although a ten-turn loop is shown in this drawing, the prototype uses two opposing single turn loops for balanced signal detection. Longitudinal slots in the beam pipe permit penetration of the axial magnetic field into the flux conserving volume, while shielding the beam from transverse fields that could cause RF beam motion due to cavity modes. Relevant dimensions are listed in Table I.

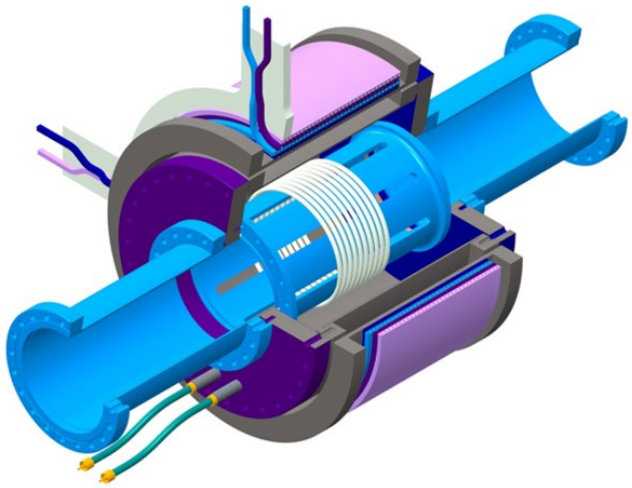

Fig. 2: Prototype DML apparatus. The bias solenoid is shown in purple. The beam pipe is shown in blue, and the flux conserving outer wall in grey Balanced-loop signal output cables are shown in green.(Adapted from ref. [10]) .

Table I. Prototype DML Apparatus Dimensions [10].

Element	Symbol	Units	Value
Beam Pipe			
Inner Radius	R_{in}	cm	7.3
Outer Radius	R_{out}	cm	7.94
Slots	N_S		8
Slot Length	L_S	cm	25.4
Slot Width	w_S	cm	1.27
Sensing Can			
Inner Radius	R_W	cm	14.92
Length	L_W	cm	30.48
Flux Loop			
Radius	R_L	cm	7.918

IV. Calibration

Our preferred method uses long, small-diameter coils driven by a high-voltage, short-pulse generator to provide the excluded flux. The excluded flux was directly measured with a loop tightly wrapped around the coil. The calibration factor is calculated from direct flux measurements [10]

$$k_{DML} \equiv \left| \Delta\Phi_{Loop} / \Phi_x \right| \tag{15}$$

Due to the non-ideal geometry of the real apparatus this measured factor deviates from the factor for an ideal coaxial geometry of infinite length

$$k_{DML} = 1 - A_{loop} / A_{Wall} \tag{16}$$

The ideal factor calculated from the dimensions in Table 1, which are taken from ref. [10], is $k_{DML} = 0.72063$.

The response of the DML to a given excluded flux can be calibrated independently of the bias magnetic field, as can be seen by setting $B_0 = 0$ in deriving Eq. (6), and we performed calibrations with and without the bias field. Based on measurements using coils with diameters, the average measured calibration factor was $k_{DML} = 0.655 \pm 1.7\%$ for our prototype [10]. This is a 10% departure from Eq. (17), largely due to the non-ideal apparatus geometry.

We undertook a number of numerical experiments to better understand the factors contributing to the departure from ideal in an effort to assess the overall uncertainty that can be expected in upcoming beam measurements at DARHT.

V. SIMULATIONS

The preceding derivation assumed an infinitely long system. Although in practice the beam might fit this model, the diagnostic apparatus certainly does not. In fact, the measured calibration constant is 10% less than the ideal calculated from Eq.(6). Therefore, Eq.(6) must be corrected to account for the finite length of the flux conserving can. .Moreover, the pulsed coils used for calibration were also of finite length. In order to investigate these corrections, we resorted to magnetic field simulations.

The PerMag magnetic field solver was used to simulate calibration of the DML [11, 12] . These simulations are 2D. The PerMag postprocessor simplifies the required flux calculations by providing the magnetic vector potential $rA_\theta = \Phi / 2\pi$, where Φ is the flux linking a disk with radius r. Perfect conductor flux conserving surfaces are modeled by imposing Dirichlet boundary conditions. The calibration coil is modeled as a thin current sheet, instead as a helix. The error introduced by this approximation will be assessed in future work with 3D simulations.

A. Ideal Infinite Geometry

In order to establish the accuracy of numerical experiments, one must begin with simulations of a problem with a known analytic solution. For the DML, this baseline was a very long coil in a very long pipe to quantify the numerical error when compared to the analytic expression from Eq. (6). These DML numerical experiments began with a simulation of a 150-cm long calibration coil with a 1.255-cm radius in a 200-cm long pipe with 15-cm inner radius. Zoning was reduced until an accuracy greater than 1% was achieved.

Fig. 3 and Fig. 4 show the results of this simulation. The simulated calibration factor was $k_{DML} = 0.755235$ calculated for a loop with radius $R_{Loop} = 7.5$ cm . Compared with the exact value 0.75 from Eq. (6), this is in error of only 0.7%, which is competitive with the best physical measurements.

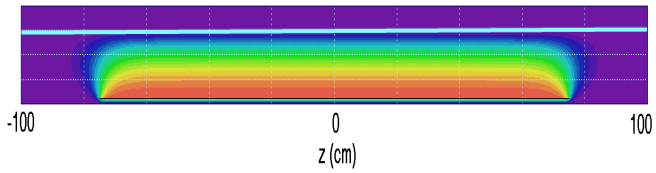

Fig. 3: rA_θ outside of a 150-cm long calibration coil in a 200-cm long flux conserving pipe (wall shown in cyan). Color is graded from zero (blue) to maximum (red).

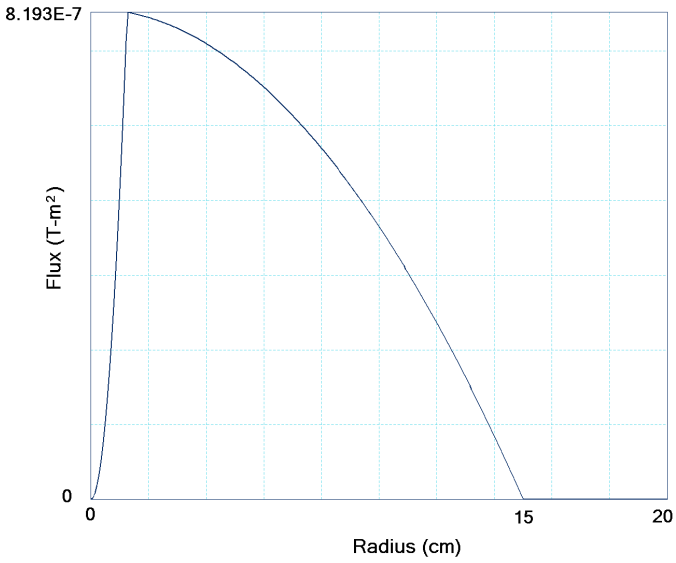

Fig. 4: Magnetic flux ($2\pi rA_\theta$) at z=0.

B. Calibration Coil Finite Length

The next simulation investigated the effect of finite length of the calibration coil. For this, the length was shortened to that used in the laboratory calibrations, 45 cm [10]. Plots similar to Fig. 3 and Fig. 4 were obtained, but not reproduced here in the interest of brevity. The simulated calibration factor obtained by analysis of the data was 0.75238, a reduction of less than 0.38% from the previous result, and only 0.31% greater than the ideal 0.75, suggesting that errors in coil length alone would contribute insignificant uncertainty to our calibrations.

C. Outer Wall Finite Length

Simulations to investigate the effect of non-uniform outer wall used the 150-cm coil length of the baseline described in section V.A. The 30-cm ID outer wall was necked down to the 14.6-cm beam pipe ID at either end of the 30.48-cm length of the can, as shown in Fig. 5 . The simulated calibration factor from this simulation results was $k_{DML} = 0.733771$, which is only 2.21% less than for an infinite uniform geometry (0.75). Thus, the finite length of the outer wall appears not to significantly reduce the sensitivity of the DML.

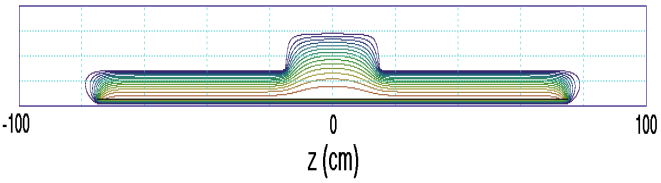

Fig. 5: Magnetic field in flux conserving beam tube and DML apparatus.

D. Combined Finite Length Effects

The final simulation with these dimensions combined the short coil with the finite length can. Fig. 6 shows the central 60 cm of the magnetic field in this configuration. The simulated calibration factor from this result was $k_{DML} = 0.733577$, which is only 0.03% less than that for a long coil with this wall geometry. The combined effect of finite length reduces the ideal factor (0.75) by only 2.2%.

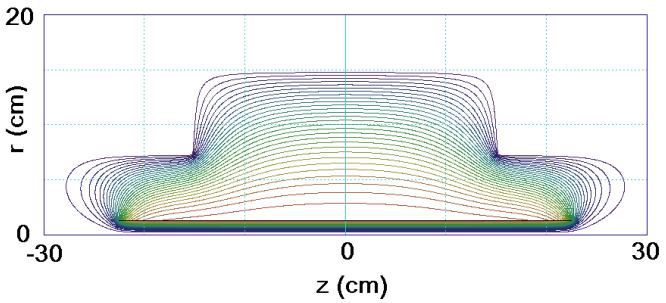

Fig. 6: Magnetic field of calibration coil in flux conserving can (60 cm of a 200-cm long simulation shown).

E. As-Built Simulations

The simulation of the last paragraph was repeated with as-built dimensions (Table I) [10]. The simulated calibration factor using as-built dimensions is $k_{DML} = 0.70125$, which is 2.4% less than the ideal factor (0.71836) calculated for the same dimensions.

Finally, the DML apparatus was actually calibrated without the beam pipe extensions shown in Fig. 2. The magnetic field for the calibration configuration is shown in Fig. 7. The simulated calibration factor in this configuration is $k_{DML} = 0.70065$, which is only 0.09% different than with the beam pipe extensions attached. Thus leaving the beam pipes off, as was done for the calibration experiments, has little affect on the results.

This simulation is the most accurate 2D model of the calibration experiments and its results differs from the measured value (0.655 [10]) by 7%. This difference is tentatively ascribed to 3D effects, measurement data, and analysis. 3D simulations are needed to further narrow down the reason.

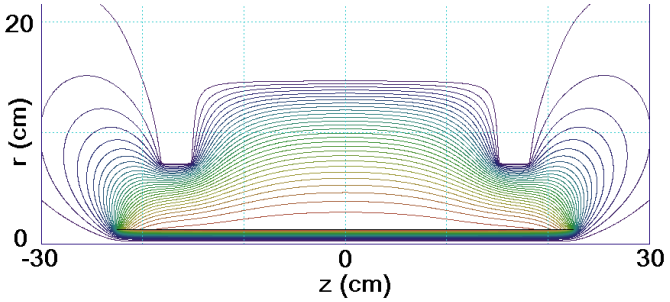

Fig. 7: Magnetic field of calibration coil in DML apparatus as calibrated.

Results of these 2D simulations are summarized in Table II.

Table II. Simulated Calibration Factors

Geometry	k_{DML} **(Eq. 6)**	k_{DML} **(simulated)**	**Diff %**	k_{DML} **(measured)**	**Diff %**
Infinite:	0.75000				
Long Coil		0.75523	0.70		
Short Coil		0.75238	0.32		
Can+Pipe:					
Long Coil		0.73377	2.16		
Short Coil		0.73358	2.16		
As- Built:	0.71836			**0.655**	**9.67**
With Pipe		0.70125	2.38		
Bare Can		0.70065	2.47	**0.655**	**6.97**

F. 3D Effects

Simulation of three dimensional effects is beyond the scope of this article. However, these effects deserve some discussion, because they can introduce further uncertainty into the calibrations. The two most obvious 3D effects are the non-ideal helix of the calibration coils, and the slotted beam tube.

The excluded flux of a loosely wound helix differs from the uniform current sheet assumed in this article. There are approximations for this [13], as well as an exact analytic solutions [14, 15] . These can be used to calculate the helical correction for an ideal, infinite length geometry. In this case, the magnetic field produced by the helical coil inside a flux conserving tube can be calculated by the method of images. To do this, one superimposes the field of an image coil placed outside the tube in order to meet the boundary conditions at the tube wall ($B_r = 0$), and flux conservation ($R_W A_\theta = 0$). The exact analytic expressions are Bessel expansions for the magnetic vector potential, so the flux ratio needed for calibration can be readily obtained from rA_θ calculated for the coil plus its image. However, 3D simulations would be needed to properly include the finite length effects.

VI. Conclusions

These 2D simulations help quantify how the finite length of our apparatus reduces its sensitivity from the ideal. This is evidenced by the reduction of the calibration factor from its value for an infinite length geometry. Furthermore, the simulations show that there is little accuracy to be gained by lengthening the calibration coils beyond what we used for the calibrations, and that difference in lengths of the coils we used adds less than 0.5% uncertainty to the results.

Although 2D simulations are useful for clarifying finite length effects, they are inadequate for predicting the calibration constant measured for our DML apparatus to an accuracy better than 7%.. This must be addressed with 3D modeling, and future directions include calculations of the correction for the helicity of the calibration coils, Simulations of measurements of a Larmor rotating beam in the field of the bias solenoid of this apparatus are also anticipated.

Of course, there are other sources of uncertainty in our calibrations, such as data recording and analysis, and will address these after isolating geometrical effects through further numerical experiments.

Acknowledgment

We are happy to acknowledge informative discussions about this topic with our colleagues.

This work was supported by the National Nuclear Security Agency of the United States Department of Energy under Contract No. 89233218CNA000001 .

References

[1] W. E. Quinn, "Measurement of plasma beta in high-beta fusion experiments," in *Diagnostics for fusion experiments*, Varona, Italy, Elsevier, 1979, pp. 433 - 446.

[2] W. E. Nexsen, R. D. Scarpetti and J. Zentler, "Reconstruction of FXR Beam Conditions," in *Part. Accel. Conf.*, Chicago, IL, USA, 2001.

[3] W. E. Nexsen, "A non-interfering beam radius diagnostic suitable for induction linacs," Lawrence Livermore National Laboratory Report UCRL-TR-213331, 2005.

[4] F. Mu, "Diamagnetic loop diagnoses emittance of intense pulse beam," in *17th Int. Conf. High Power Part. Beams*, Xian, China, 2008.

[5] C. Ekdahl, "Non-invasive measurement of electron beam size with diamagnetic loops," *Rev. Sci. Instrum.,* vol. 72, no. 7, pp. 2909 -2914, 2001.

[6] R. B. Miller, Intense charged particle beams, New York, N. Y.: Plenum Press, 1985, pp. 108, et seq..

[7] S. Humphries, Charged Particle Beams, New York: Wiley, 1990.

[8] M. Reiser, Theory and design of charged particle beams, New York. NY: Wiley, 1994.

[9] M. L. Sloan and H. L. Davis, "Design and testing of low temperature intense electron beam diodes," *Phys. Fluids,* vol. 25, no. 12, pp. 2337 - 2343, 1982.

[10] H. V. Smith, B. Broste and C. Ekdahl, "A diamagnetic-loop-based beam radius monitor," Los Alamos National Laboratory Report, DARHT Tech. Note 507, LA-UR-21-, 2021.

[11] S. Humphries, Field solutions on computers, CRC Press, 1997.

[12] S. Humphries, "Technical information: TriComp Series," Field Precision, LLC, 2013. [Online]. Available: www.fieldp.com/technical.html.

[13] F. Grover, Inductance Calculations, New York, NY, USA: Van Nostrand, 1946.

[14] S. Park and et al., "Exact magnetic field of a helical wiggler," *J. Appl. Phys.,* vol. 53, no. June, pp. 1320 - 1325, 1982.

[15] T. Tominaka, "Vector potential for a single helical current conductor," *Nucl. Instrum. Meth.,* vol. A523, pp. 1 - 8, 2004.